Loading Pattern Optimization for OPR-1000 Using Simulated Annealing with Pin-wise Vision Transformer Based Screening Technique

Seongjin Jeong [a], and Hyun Chul Lee [a*]
[a]*School of Mechanical Engineering, Pusan Natl. Univ., 2, Busandaehak-ro 63beon-gil, Geumjeong-gu, Busan, 43210*
[*]*Corresponding author: hyunchul.lee@pusan.ac.kr*

Keywords : loading pattern, optimization, simulated annealing, screening technique, vision transformer

1. Introduction

To enhance the safety and efficiency of a reactor core, it is crucial to optimize the fuel assembly loading pattern (LP). However, given the vast number of potential LPs, evaluating every possible LP is impractical. Although methods such as simulated annealing (SA) can be employed to search for an optimal solution, they still necessitate a substantial number of LP evaluations. To address this challenge, a screening technique utilizing a simplified model [1] has been proposed. This method can evaluate LPs at a much faster rate compared to traditional 3D deterministic calculations, thus enabling more rapid LP optimization.

Previous research has explored the use of Convolutional Neural Networks (CNNs) for LP evaluation [2]. However, CNNs are designed to analyze images using convolutional filters of fixed sizes, making them more suited for extracting features from relatively small regions. This characteristic of CNN limits their efficiency when dealing with large LP images where each pin is represented as a pixel.

In this study, we aim to enhance the accuracy of LP evaluations by utilizing the Vision Transformer (ViT) model [3]. ViT divides the entire image into small patches and captures the relationships between all patches using a self-attention mechanism. This process helps in extracting features over a broader range compared to the filter-based approach of CNNs. By integrating ViT, we have improved the efficiency of the screening technique, thereby enabling faster execution of SA to identify the optimal LP.

2. Description of AI Models Training

Two AI architectures, CNN and ViT, were used to develop the models. The dataset for training these models was generated using the STREAM/RAST-K 2.0 [4] code system, based on LPs of OPR-1000.

2.1 Training Dataset

The LPs for the training dataset were generated by shuffling fuel assemblies (FAs) based on the reference LP shown in Figure 1. The specifications of the fuel assemblies in the reference LP are shown in Table 1. The method for shuffling the FAs is illustrated in Figure 2. First, the FAs located at the center of the core (region 0) do not participate in the exchange. Next, FAs in region 1 and FAs in region 2 are swapped separately. If the exchange of FAs in Region II disrupts the 8th symmetry of the FA types, the symmetry is maintained by swapping the corresponding FAs in the 8th symmetric region. Finally, two FAs of identical type in region 1 are selected and exchanged with two FAs in region 2.

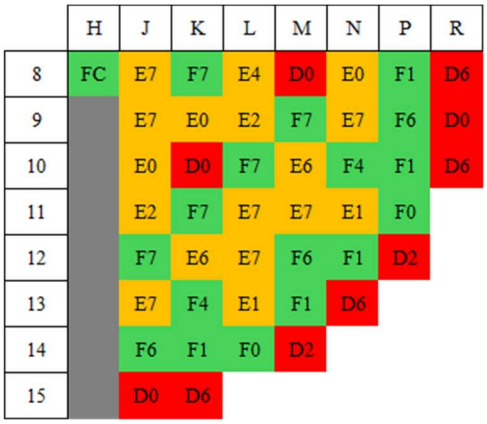

Fig. 1. The reference LP of OPR-1000 [2]. Green indicates fresh fuel, yellow indicates once-burnt, and red indicates twice-burnt.

Table I: Specifications of fuel assemblies in the reference LP [2].

FA Type	Fuel Enrichment [wt.% U-235]		No. Rods		Burnable Poison Fraction [wt.% Gd2O3]
	Normal	Zoned	Zoned	BP	
D0	4.50	4.01	52	0	-
D2	4.50	4.01	52	12	6.0
D6	4.50	4.01	52	12	8.0
E0	4.64	4.10	52	0	-
E1	4.64	4.10	52	8	6.0
E2	4.64	4.10	52	12	6.0
E4	4.64	4.10	52	16	8.0
E6	4.64	4.10	52	12	8.0
E7	4.64	4.10	52	20	8.0
F0	4.65	4.10	52	0	0.0
F1	4.65	4.10	52	8	6.0
F4	4.65	4.10	52	16	8.0
F6	4.65	4.10	52	12	8.0
F7	4.65	4.10	52	20	8.0
FC	2.20	-	0	0	-

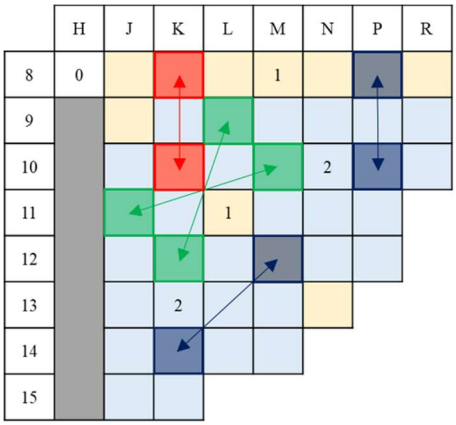

Fig. 2. The regions of LP and shuffling methods. Red indicates region 1 swapping, green indicates region 2 swapping, and blue indicates region 1 – 2 swapping.

A total of 100,000 LPs were generated. For each LP, the cycle length and peaking factor were calculated using RAST-K code. The cycle length is defined as the Effective Full Power Day (EFPD) at which the critical boron concentration reaches 10 ppm, and the peaking factor represents the maximum value of Fxy in the cycle. The distributions of the calculated cycle length and peaking factor are shown in Figure 3 and 4.

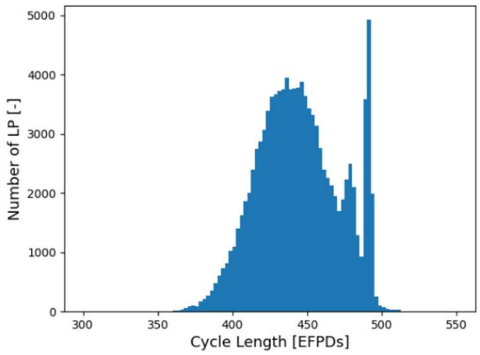

Fig. 2. Distribution of the cycle length.

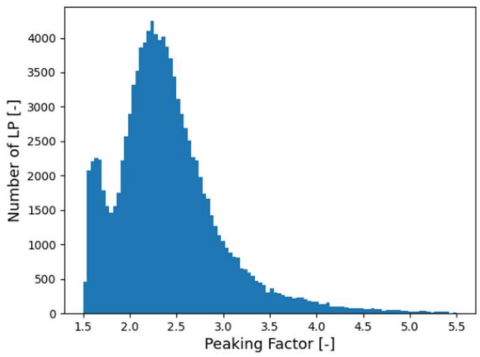

Fig. 3. Distribution of the peaking factor

The features provided to the AI models differs between the CNN and ViT approaches. For the CNN, assembly-wise data is used, which includes the average fuel enrichment, the number of BP rods, the mass fraction of burnable poison, and the initial average burnup for each assembly, as shown in Figure 3. In contrast, the ViT uses pin-wise data, which includes the fuel enrichment, mass fraction of burnable absorber, and the 4-unit assembly burnup for each pin, as illustrated in Figure 4. Based on these features, Two models were trained with each architecture, the cycle length prediction model and peaking factor prediction model. When training the models, the entire dataset was split into three portions: 80% was used for model training, 10% for validation during training, and the remaining 10% for testing the model after training was completed.

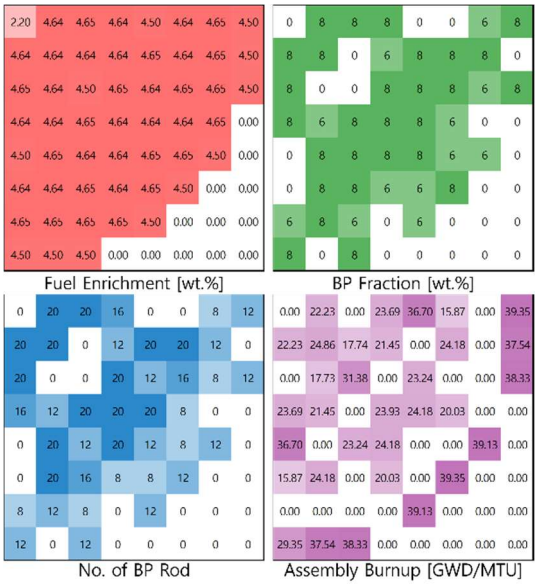

Fig. 3. Example of the features for the CNN model.

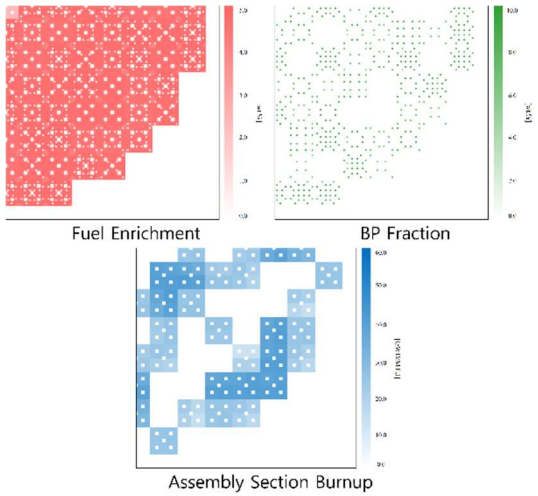

Fig. 4. Example of the features for the ViT model.

2.2 AI model Training Results

The cycle length prediction model of CNN consists of 9 convolutional layers with a total of 650K parameters. The peaking factor prediction model of CNN, on the

other hand, comprises 13 convolutional layers with a total of 1500K parameters.

The cycle length prediction model of ViT consists of 3 Transformer encoder layers with a total of 350K parameters. The peaking factor prediction model consists of 9 Transformer encoder layers, with a total of 2,100K parameters.

Both the CNN and ViT models were developed using AI modules provided by Pytorch. The detailed hyperparameters of the models are listed in Table 2.

Table II: Hyperparameters of the models

Architecture	Prediction Type	Hyperparameter	Value
CNN	Cycle Length	No. Kernel	128
		Kernel Size	3
		Stride Length	1
		No. Layer	9
	Peaking Factor	No. Kernel	256
		Kernel Size	3
		Stride Length	1
		No. Layer	13
ViT	Cycle Length	Dimension	256
		No. Head	4
		Feed-Forward Dimension	128
		No. Layer	3
	Peaking Factor	Dimension	256
		No. Head	4
		Feed-Forward Dimension	512
		No. Layer	9

Figures 6 and 7 show the RMS error between the predicted and actual values using the validation data during the training. It shows that peaking factor model using ViT architecture completes their training faster than the CNN models. Additionally, for the peaking factor, the ViT prediction model shows a lower RMS error compared to the CNN model at the point where training is completed. On the other hand, for the cycle length, both models demonstrate similar RMS error progresses.

Figures 8 and 9 compare the RAST-K calculated values with the Ai-predicted values. The two graphs for cycle length looks similar, but for the peaking factor, the predictions from the ViT model are more closely clustered around the actual values.

Fig. 6. Training convergence progress of the cycle length prediction models.

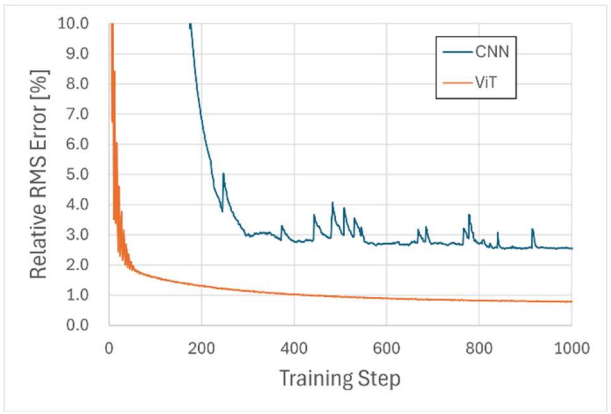

Fig. 7. Training convergence progress of the peaking factor prediction models.

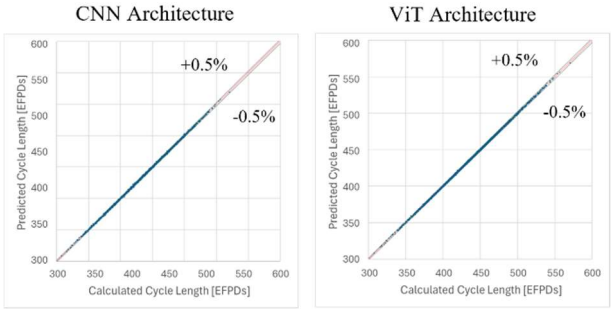

Fig. 8. Training results of the cycle length prediction models.

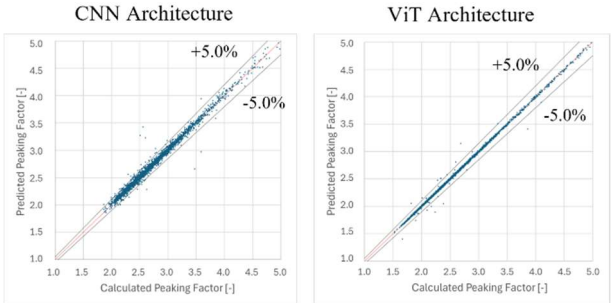

Fig. 9. Training results of the peaking factor prediction models.

Table 3 presents the relative prediction errors of each model. Consistent with the graphical results, there is almost no difference between the two models in cycle length prediction, but for the peaking factor, The ViT model exhibited a relative RMS error of 0.78%, which is significantly lower than the 2.65% of the CNN model. Additionally, the probability of the relative absolute error being within 5% was 99.8% for the ViT model, compared to 99.4% for the CNN model. The maximum relative absolute error for the ViT model was also lower, at 18.90%, compared to 36.37% for the CNN model.

Table III: Prediction error of the models.

Prediction Type	Architecture	Relative Prediction Error [%]		
		RMS	Abs.	Max. Abs.
Cycle Length	CNN	0.12	99.8 (Abs. < 0.5%)	0.87
	ViT	0.12	99.3 (Abs. < 0.5%)	0.89
Peaking Factor	CNN	2.65	99.4 (Abs. < 5.0%)	36.37
	ViT	0.78	99.8 (Abs. < 5.0%)	18.90

3. Simulated Annealing with Screening Technique

3.1 Multi-Objective Simulated Annealing

In the LP optimization problem, it is necessary to satisfy both the cycle length and peaking factor limits. To achieve this, Multi-Objective Simulated Annealing (MOSA) was applied [1]. The objective functions for cycle length and peaking factor are defined in Equations 1 and 2, respectively. In the equations, $\overline{CYC}$ and $\overline{PF}$ represent the average cycle length and peaking factor from the training data, while CYC_{lim} and PF_{lim} are the design limit values for the OPR-1000, set at 492 EFPDs and 1.60. These two functions are then combined into a multi-objective function for the LP, as shown in Equation 3.

$$(1)\ J_{CYC}(X) = \begin{cases} 1 + \frac{1}{\overline{CYC}}(CYC(X) - CYC_{lim})^2, \\ \quad when\ CYC(X) < CYC_{lim} \\ 0, \\ \quad when\ CYC(X) > CYC_{lim} \end{cases}$$

$$(2)\ J_{PF}(X) = \begin{cases} 1 + \frac{1}{\overline{PF}}(PF(X) - PF_{lim})^2, \\ \quad when\ PF(X) < PF_{lim} \\ 0, \\ \quad when\ PF(X) > PF_{lim} \end{cases}$$

$$(3)\ J(X) = J_{CYC}(X) + J_{PF}(X)$$

In the SA process, an initial LP is selected randomly, and small perturbations are applied to generate new LPs. These perturbations involve swapping fuel assemblies within the core, while maintaining the overall symmetry of the core configuration. The MOSA algorithm evaluates each new LP using the combined objective function, and the AI-based screening technique rapidly predicts the cycle length and peaking factor for each candidate LP.

The acceptance of a new LP depends on whether it improves the objective function or is accepted probabilistically based on the SA schedule. This allows the algorithm to explore a wide solution space while avoiding local minima. The process continues until a termination criterion is met, such as a set number of iterations or a negligible improvement in the objective function over a series of iterations.

3.2 Screening Technique Assisted by AI Model

The screening technique plays a critical role in enhancing the efficiency of the SA process. By utilizing the AI models trained on CNN and ViT architectures, the technique rapidly evaluates candidate LPs, significantly reducing the computational cost compared to full 3D deterministic calculations.

However, since AI predictions inherently have some error compared to actual values, this must be considered. For the LPs used in training, the average error ($\overline{\Delta J}$) and standard deviation (σ) of the objective function are calculated by comparing the AI-predicted values with the RAST-K calculated values. These values are then used to define the range within which the true objective value of the current LP may exist. The upper ($J^{3D}_{max}(X)$) and lower ($J^{3D}_{min}(X)$) bounds of this range are determined by Equations 5 and 6.

$$(5)\ J^{3D}_{max}(X) = J^{AI}(X) + \overline{\Delta J} + 2\sigma$$

$$(6)\ J^{3D}_{min}(X) = J^{AI}(X) + \overline{\Delta J} - 2\sigma$$

If the upper bound of the current LP is lower than the acceptable value, the LP is accepted. Conversely, if the lower bound is higher than the acceptable value, the LP is rejected. If the acceptable value lies within these bounds, a 3D calculation is performed.

3.3 Result

Table 4 presents the average results of 20 runs each for CNN-based SA and ViT-based SA. In the case of SA using CNN, the average efficiency was 99.6%, while the efficiency slightly increased to 99.8% when using the ViT. This improvement in efficiency can be attributed to the more accurate peaking factor prediction model used in the ViT-based approach.

Table 5 shows the average optimal LP in the SA results. the cycle length and peaking factor of the

Optimal LP showed almost no difference between the two approaches. This is likely because the AI models have trained with a little of LPs near of the optimal points, which causes the accuracy of the model prediction lower.

Table IV: Average of SA results.

AI model	No. of LP evaluations			Efficiency [%]
	RAST-K	AI	Total	
CNN	148	38962	39110	99.6
ViT	99	50570	50669	99.8

Table V: average optimal LP in the SA results.

AI Model	Cycle Length [EFPDs]	Peaking Factor [-]
CNN	495.5	1.590
ViT	496.1	1.592

4. Conclusions

This study developed an ViT-assisted screening technique to enhance the efficiency of SA for optimizing the LP of the OPR-1000 reactor. Comparing CNN-based and ViT-based approaches, the ViT model showed a slight improvement in efficiency (99.8% vs. 99.6%) due to more accurate predictions, especially for the peaking factor. Both approaches yielded similar optimal LPs, indicating that the AI model need more data nearing the optimal LP.

In future research, we plan to incorporate the optimal LP obtained through SA into the AI training dataset, aiming to develop models capable of performing more accurate evaluations in the vicinity of the optimal LP region. By adding more data near the optimal region compared to the existing dataset, the AI will be able to focus on additional learning in that area, leading to more precise LP evaluations. This approach is also expected to enhance the efficiency of the screening technique in the SA process, allowing for the discovery of more optimal LPs in a shorter time frame.

REFERENCES

[1] T. K. Park, H. G. Joo, and C. H. Kim, Multiobjective Loading Pattern Optimization by Simulated Annealing Employing Discontinuous Penalty Function and Screening Technique, Nuclear Science and Engineering, Vol.162, p. 134-147, 2009.

[2] H. Jang, H. C. Shin, D. Kim, and H. C. Lee, Application of Convolutional Neural Network to Fuel Loading Pattern Optimization by Simulated Annealing, Transactions of the Korean Nuclear Society Virtual Autumn Meeting, 2020

[3] A. Dosovitskiy, L. Beyer, A. Kolesnikov, Et Al., AN IMAGE IS WORTH 16X16 WORDS: TRANSFORMER FOR IMAGE RECOGNITION AT SCALE, ICLR, 2021.

[4] J. Park, J. Jang, H. Kim, Et Al., RAST-K v2- Three Dimensional Nodal Diffusion Code for Pressurized Water Reactor Core Analysis, Energies, 13: 6324, 2020.